Experimental Thermal and Fluid Science 51 (2013) 342–353

Contents lists available at ScienceDirect

Experimental Thermal and Fluid Science

journal homepage: www.elsevier.com/locate/etfs

Off-axis PTV for 3-D visualization of rotating columnar flows

Yuichi Murai [a,*], Jozef H.A. Vlaskamp [b], Yuichi Nambu [a], Takahiro Yoshimoto [a], Mark A. Brend [c], Petr Denissenko [b], Peter J. Thomas [b]

[a] Laboratory for Flow Control, Faculty of Engineering, Hokkaido University, Sapporo, Japan
[b] Fluid Dynamics Research Centre, School of Engineering, University of Warwick, Coventry, UK
[c] Department of Aeronautical and Automotive Engineering, Loughborough University, Loughborough, UK

ARTICLE INFO

Article history:
Received 13 March 2013
Received in revised form 19 July 2013
Accepted 19 August 2013
Available online 27 August 2013

Keywords:
Rotating flow
Particle tracking velocimetry
Taylor-Column
Wake
Flow visualization

ABSTRACT

A new simple optical method for visualizing flow structures generated in a rotating flow is presented. The method consists of planar PTV with sheet illumination slightly offset to the rotation axis and a geometric reconstruction of velocity vector field under the assumption of azimuthal periodicity. Two types of columnar flows intrinsically associated with rotating flows are investigated with the method. The two types of flow are a local columnar wake induced behind a moving sphere, and an asymmetrically precessing Taylor Column created below a spinning disk. By means of this new technique we obtain the first quantitative visualization of the columnar wake and the three-dimensional structure of the Taylor Column.

1. Introduction

Rotating flows are ubiquitous in science and engineering. In such flows Coriolis forces give rise to phenomena absent in non-rotating flows [6,22,4]. These phenomena can appear counterintuitive to anyone not familiar with the theoretical background of rotating flows. One example is, for instance, the Taylor-Proudman theorem derived from the geostrophic approximation of the full momentum equation [17,20,6,21,4]. For a fluid rotating with angular velocity Ω that is aligned with the x-axis of a Cartesian coordinate system (*cf.* Fig. 1) fixed in the rotating frame of reference the Taylor-Proudman theorem states that the effects of Coriolis forces are such that the derivatives $\partial v/\partial x$ and $\partial w/\partial x$ of the velocity components v and w in the y and z coordinate directions are identically zero. This means that when there exists a flow field $v(y,z)$, $w(y,z)$ at a plane $x = x_1$ then the flow field must be the same at any other plane $x = x_2$. This requirement gives rise to the formation of a cylindrical flow that is aligned with the axis of rotation referred to as a Taylor-Column. The phenomenon has received attention in the fields of geophysical flows and turbo machinery and represents one striking manifestation of the action of the Coriolis forces present in rotating fluids.

In this study two kinds of flow which display such a columnar structure are investigated. One is flow around a sphere that propagates along the axis of rotation. A Taylor-Column will develop ahead of the sphere and in its wake as first described by Maxworthy [12], Maxworthy [13]. The flow scenario is similar to that observed for vortex rings in a rotating fluid [3]. We investigate Reynolds numbers $O(10^3)$ as this is the regime where a single toroidal vortex is known to form behind the sphere in a non-rotating quiescent fluid during the phase immediately following an impulsive start of the sphere motion (see e.g. [10,18,11]). Experiments were conducted for a range of Rossby numbers to investigate the dynamics in the flow regime where the axial and the circumferential momentum compete with each other. The second flow structure considered is a Taylor-Column that is created with a disk rotating differentially to the background rotation. The present study focuses on how such a two-dimensional column departs into a three-dimensional structure as parameters change. The origin of such three-dimensionality is discussed in comparison with dye-visualization experiments of Hide and Titman [7].

Particle image velocimetry (PIV) has been a powerful tool for studying three-dimensional flows in rotating fluids. Norman et al. [16] showed various three-dimensional wake patterns of a sphere with a surface protrusion rotating in the azimuthal direction. Foster and Munro [5] visualized unique circulation structures in a stratified fluid inside a square container during the linear spin-up of the system. In the present study we introduce particle tracking velocimetry (PTV) as a new technique to reconstruct the three-component velocity-vector field from recordings made by a

* Corresponding author. Address: Laboratory for Flow Control, Faculty of Engineering, Hokkaido University, N13W8, Sapporo, Hokkaido 060-8628, Japan. Tel.: +81 11 706 6372.
E-mail address: murai@eng.hokudai.ac.jp (Y. Murai).

0894-1777/$ - see front matter © 2013 Elsevier Inc. All rights reserved.
http://dx.doi.org/10.1016/j.expthermflusci.2013.08.017

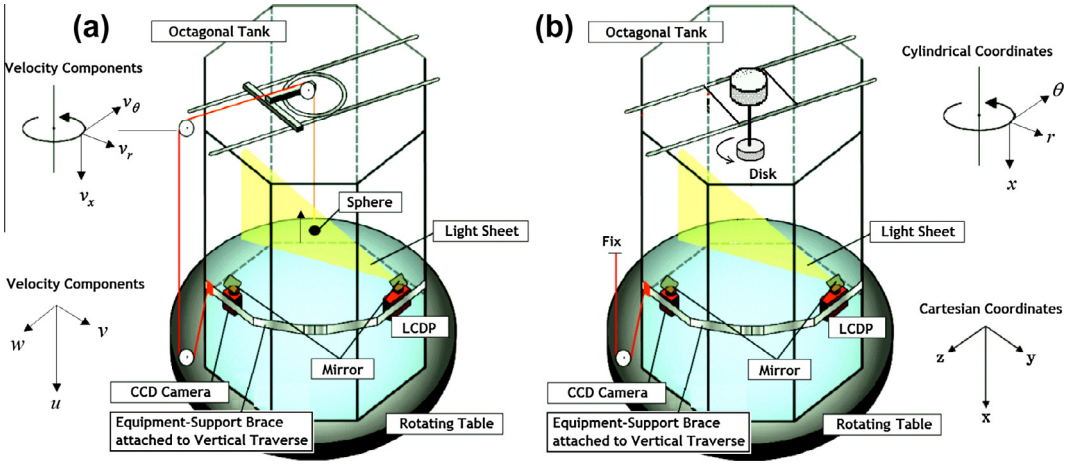

Fig. 1. The experimental setup: (a) for sphere wake measurement, (b) for Taylor Column measurement.

single camera together with a light sheet that is slightly offset from the axis of the rotation. The technique is suitable for detecting, for instance, columnar swirling flow structures arising from the Coriolis forces associated with the background rotation. In comparison with multi-camera 3D PTV or PIV methods our new methodology is substantially less technologically challenging to integrate into any experimental configuration. This is in particular the case when the entire experimental arrangement has to be mounted, for instance, on a rotating turntable. The first half of the present study outlines the principle of our new off-axis PTV methodology by summarizing the relevant underlying theoretical issues. Thereafter we illustrate two typical applications of the method by discussing results obtained with our new method for flow around a sphere and within a Taylor Colum in a rotating flow.

2. Experimental facility

Experiments were conducted using the large rotating-tank facility at the University of Warwick. Fig. 1 displays an overview of the experimental rig. The setup consists of a large water-filled tank of 2.5 m height with octagonal horizontal cross section of 1 m wide. The tank is mounted on top of a computer-controlled rotating turntable[1].

For experiments of sphere's wake, a test sphere is mounted such that its centre coincides with the central axis of the tank as illustrated in Fig. 1(a). The sphere has a diameter of 50 mm and is supported by a thin thread, by means of which it can be pulled upwards along the central, vertical axis of the tank. A computer-controlled vertical traverse on the outside of the tank enabled mounting the required PTV equipment such as a CCD camera (Panasonic, HDC-SD1-S) and an illumination device (liquid crystal display projector, Panasonic, TH-LB10NT) to generate a suitable light sheet inside the tank via an arrangement of tilted mirrors. The thickness of the light sheet is computer-controlled, and the width was 5 pixels of the whole image size of 1024 × 768 pixels, which is equivalent to about 5 mm thickness in the flow. The total power of the light source is 200 W, of which a small portion is contained as useful power in the measurement plane. The light sheet thickens with the distance from the source due to diverging effect of the light projection. However, this thickening effect is negligible on the scale of the measurement window relative to the characteristic length scale of the flow. Moreover, a slightly-out-of-focus condition of the projected light at the measurement plane, was adopted to avoid particle flickering that results from the interference of light originating from individual pixels of pixel ensembles.

The thread supporting the sphere is mechanically connected to the equipment-support brace on the vertical traverse by means of a system of pulleys as shown in the figure. This ensures that the sphere and the light sheet and camera move in phase. Hence, the PTV system captured data within the rotating and linearly traversing frame of reference. The seeding material used for our PTV measurements is Talisman 30 which is a polymer powder with specific gravity 0.99 and diameters in the range of 100–200 μm. Following the initial spin-up of the turntable the water inside the tank was allowed to settle for at least 12 h, to reach a state of rigid-body rotation, before experiments commenced.

For the experiments on the long Taylor-Column, the disk is set at the center coaxially with the rotating water tank as shown in Fig. 1(b). The rotational speed of the disk is independently controlled to investigate the influence of the magnitude and sign of the differential rotation. By traversing the equipment-support brace, similar to the experiments using the sphere, we visualize and measure the whole 3-D structure of Taylor-Column with the off-axis PTV.

3. Wake of moving sphere in background rotation

A moving sphere induces a wake behind it, and its flow structure can be described with a Reynolds number as reported by numerous papers to date (see for example [1,19]). When it moves in a rotating fluid, the wake structure changes completely due to presence of Coriolis forces, as governed by the Rossby and Reynolds numbers. These are defined by

$$Re = \frac{UD}{\nu}, \quad Ro = \frac{U}{2\Omega D} \tag{1}$$

where U and D represent, respectively, the translational velocity and the diameter of the sphere, Ω is the angular velocity of the background rotation, and ν is the kinematic viscosity of the water inside the tank. We use the inverse of the Rossby number, Ro^{-1}, to enable characterizing data for the non-rotating flow ($\Omega = 0$) by the finite value $Ro^{-1} = 0$. The detailed experimental conditions are summarized in Table 1.

At low Ro number or high Ro^{-1} number, the wake forms an axisymmetric columnar structure which has a significant velocity component in the azimuthal direction. We measure such a flow structure positioning the light sheet of the PTV system slightly offset from the rotational axis of the tank as elaborated below.

[1] Photographs of the facility can be accessed at www.eng.warwick.ac.uk/staff/pjt/turntabpics/voriskt.html.

Table 1
Summary of the experimental conditions for sphere wake measurement.

Towing speed	U	5–100	(mm/s)
Sphere diameter	D	50	(mm)
Rotating speed	Ω	0.00, 0.26, 0.52	(rad/s)
Reynolds number	$\mathrm{Re} = UD/\nu$	$0.25–5.0 \times 10^3$	(–)
Rossby number	$Ro = U/(2\Omega D)$	0.10–3.82	(–)
Light sheet thickness		5 (effectively 3 mm)	(mm)
Light sheet off-set	ε	5	(mm)
Frame rate for PTV		30	(fps)
Shutter speed		120	(1/s)
Image size		1920×1080	(pixels)
Spatial resolution		0.070	(mm/pixel)

3.1. Principle of off-axis PTV or axisymmetric flow measurement

Fig. 2 illustrates the measurement configuration and defines the nomenclature used. The velocity vector at a point within the light sheet is referred to as $\mathbf{V}_1$. Due to the axisymmetry of the flow field with respect to the vertical x axis, the relationship between $\mathbf{V}_1$ and the velocity vector $\mathbf{V}_2$ at equal radius, r, from the center is given by

$$\mathbf{V}_2 = \mathbf{A}\cdot\mathbf{V}_1, \mathbf{A} = \begin{bmatrix} 1 & 0 & 0 \\ 0 & \cos\theta & -\sin\theta \\ 0 & \sin\theta & \cos\theta \end{bmatrix}, \mathbf{V}_1 = \begin{pmatrix} u_1 \\ v_1 \\ w_1 \end{pmatrix}, \mathbf{V}_2 = \begin{pmatrix} u_2 \\ v_2 \\ w_2 \end{pmatrix} \tag{2}$$

where $\mathbf{A}$ denotes the rotation tensor around the x axis, and θ is the angle between the two circumferential points. The above equation yields two relationships between the velocity components v and w:

$$w_1 \sin\theta = v_1 \cos\theta - v_2, \tag{3}$$

$$w_2 \sin\theta = v_1 \sin^2\theta + w_1 \sin\theta\cos\theta = v_1 - v_2\cos\theta. \tag{4}$$

The components v_1 and v_2, in the y-coordinate direction, are in-plane velocities of the light sheet and are given by the PTV measurements directly. Using Eqs. (3) and (4), the velocity components w_1 and w_2 normal to the PTV plane, can be obtained at two symmetric points. The remaining velocity components u_1 and u_2, in the direction of the vertical x-coordinate are also in-plane components and are given directly by the collected PTV data. Hence, all three velocity components at both points are known and given by

$$\begin{pmatrix} u_1 \\ v_1 \\ w_1 \end{pmatrix} = \begin{pmatrix} u_1(from\ PTV) \\ v_1(from\ PTV) \\ (v_1\cos\theta - v_2)/\sin\theta \end{pmatrix}, \quad \begin{pmatrix} u_2 \\ v_2 \\ w_2 \end{pmatrix} = \begin{pmatrix} u_2(from\ PTV) \\ v_2(from\ PTV) \\ v_1/\sin\theta - v_2/\tan\theta \end{pmatrix}. \tag{5}$$

It is noted that the three velocity components are defined in the reference frame of the off-axis PTV plane. The same velocity components in cylindrical coordinates centered on the rotational axis are given by

$$\begin{pmatrix} v_r \\ v_\theta \\ v_x \end{pmatrix} = \begin{pmatrix} v_1\cos\alpha + w_1\sin\alpha \\ -v_1\sin\alpha + w_1\cos\alpha \\ \frac{u_1+u_2}{2} \end{pmatrix} = \begin{pmatrix} v_1\left(\frac{\sin\alpha}{\tan\theta} + \cos\alpha\right) - v_2\frac{\sin\alpha}{\sin\theta} \\ v_1\left(\frac{\cos\alpha}{\tan\theta} - \sin\alpha\right) - v_2\frac{\cos\alpha}{\sin\theta} \\ \frac{u_1+u_2}{2} \end{pmatrix}, \tag{6}$$

where v_r, v_θ, and v_z are the velocity components in the radial, circumferential, and axial directions. Here α denotes the angle from the on-axis plane as illustrated in Fig. 2 with $2\alpha + \theta = \pi$. Furthermore, α can be replaced by the offset distance ε such that the velocity components can also be expressed as

$$\begin{pmatrix} v_r \\ v_\theta \\ v_x \end{pmatrix} = \begin{pmatrix} \frac{1}{2\cos\alpha}(v_1 - v_2) \\ \frac{v_2}{2\sin\alpha} - \left(\frac{\cos\alpha}{\tan 2\alpha} + \sin\alpha\right)v_1 \\ \frac{1}{2}(u_1 + u_2) \end{pmatrix}, \quad \begin{cases} \sin\alpha = \frac{\varepsilon}{r} \\ \tan^2\alpha = \frac{(\varepsilon/r)^2}{1-(\varepsilon/r)^2} \\ r = \sqrt{\varepsilon^2 + y^2} \end{cases} \tag{7}$$

The instantaneous spatial distributions of the three velocity components are given as functions of the radial and axial coordinates r and z when the in-plane velocity-vector components v_1 and v_2 are measured within the corresponding area in the y–z plane. Thus, the present off-axis configuration constitutes a three-component two-dimensional measurement of the velocity-vector field by means of single-camera single-plane PTV. As can be seen from the expression for $\tan\alpha$ in Eq. (7) velocities in the central region $r < \varepsilon$ cannot be resolved. Indeed, the light sheet does not span the central area, so velocity there is obtained by interpolation. The flow in this central area is interpolated linearly from the velocity in the surrounding region.

The error-propagation characteristics in the reconstruction process are estimated from Eq. (7) analytically by considering perturbations in the measured velocity components, u_1, u_2, v_1, v_2, and also a small displacement error in the off-set, ε, as described in the following general form,

$$\begin{aligned} \begin{pmatrix} \Delta v_r^2 \\ \Delta v_\theta^2 \\ \Delta v_x^2 \end{pmatrix} &= \begin{pmatrix} \left|\frac{\partial v_r}{\partial v_1}\Delta v_1\right|^2 + \left|\frac{\partial v_r}{\partial v_2}\Delta v_2\right|^2 + \left|\frac{\partial v_r}{\partial \varepsilon}\Delta\varepsilon\right|^2 \\ \left|\frac{\partial v_\theta}{\partial v_1}\Delta v_1\right|^2 + \left|\frac{\partial v_\theta}{\partial v_2}\Delta v_2\right|^2 + \left|\frac{\partial v_\theta}{\partial \varepsilon}\Delta\varepsilon\right|^2 \\ \left|\frac{\partial v_x}{\partial u_1}\Delta u_1\right|^2 + \left|\frac{\partial v_x}{\partial u_2}\Delta u_2\right|^2 \end{pmatrix} \\ &= \begin{pmatrix} \frac{1+\tan^2\alpha}{4}(\Delta v_1^2 + \Delta v_2^2) + \left|\frac{\partial v_r}{\partial \varepsilon}\Delta\varepsilon\right|^2 \\ \left(\frac{\cos\alpha}{\tan 2\alpha} + \sin\alpha\right)^2\Delta v_1^2 + \frac{\Delta v_2^2}{4\sin^2\alpha} + \left|\frac{\partial v_\theta}{\partial \varepsilon}\Delta\varepsilon\right|^2 \\ \frac{1}{4}(\Delta u_1^2 + \Delta u_2^2) \end{pmatrix}. \end{aligned} \tag{8}$$

Due to combinations of trigonometric functions in each term, the error magnification factors to the velocity components dynamically change depending on the angle α. The equation expresses that the radial velocity v_r remains accurate at small angles α while

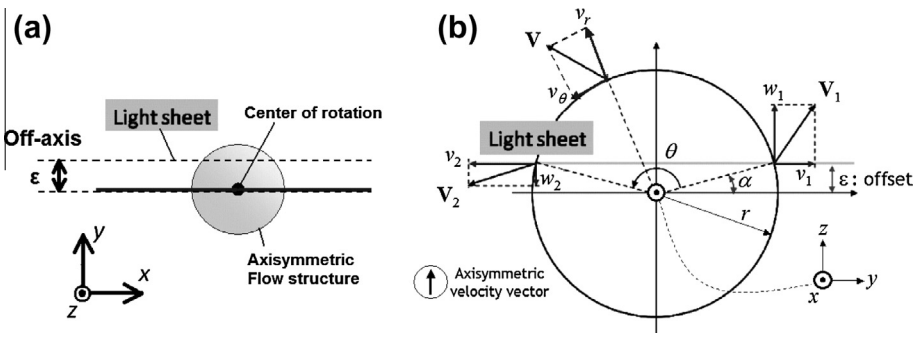

Fig. 2. Relationship between the in-plane velocity components of the off-axis PTV and the velocity vectors in the axisymmetric flow field.

the circumferential velocity v_θ requires a large angle to avoid amplified errors. In turn, the error propagation due to the off-set error, ε, have complex forms. Their impacts are given by

$$\frac{\Delta v_r}{v_r} = \frac{1}{v_r}\left(\frac{\partial v_r}{\partial \varepsilon}\Delta\varepsilon\right) = \sin^2\alpha(1-2\sin^2\alpha)\cdot\frac{\Delta\varepsilon}{\varepsilon}, \tag{9}$$

$$\frac{\Delta v_\theta}{v_\theta} = \frac{1}{v_\theta}\left(\frac{\partial v_\theta}{\partial \varepsilon}\Delta\varepsilon\right) = -\frac{1}{\cos^2\alpha}\cdot\frac{1+\frac{1}{\sin^2\alpha}\left(\frac{1}{2}-\cos\alpha\right)}{1-\frac{1}{2}\cos 2\alpha-\sin^2 2\alpha}\cdot\frac{\Delta\varepsilon}{\varepsilon}, \tag{10}$$

where Eq. (10) is valid only in the case $v_1 = v_2$. Eq. (9) illustrates that the error magnification factor, $\Delta\varepsilon/\varepsilon$, is always less than unity. In contrast, Eq. (10) indicates that the factor can increase to plus or minus infinity as $\alpha = 0$ or $\alpha = \pi/2$ but it takes zero at $\alpha = 0.193\pi$ (36.6°).

There are two main requirements as regards the geometrical setup of the present off-axis PTV. One is to reduce the off-axis displacement ε so that invisible region around the rotating axis can be minimized. The other is to thicken the light sheet such that the velocity vectors can be measured correctly even with large out-of-plane velocity components. To satisfy both conditions simultaneously, the ratio of the thickness of the light sheet to the off-axis distance ε cannot be reduced below the value of current setup shown in Tables 1 and 2. It is, nevertheless, noted that the "effective thickness" of the light sheet in our PTV setup considered here is smaller than the value described in the table because of several reasons, which are the beam divergence effect, the defocusing effect, and the threshold effect in particle detection of PTV.

The measurement principle outlined above is valid when the assumption of axisymmetric flow is appropriate. In general it is highly preferable to confirm that the flow is axisymmetric prior to conducting PTV measurements. However, there are two methods available that can be applied after the measurements to confirm axisymmetric flow. One method involves calculating the difference $u_1 - u_2$ which will be identical zero in the case of perfect axisymmetric flow (see Eqs. (6) and (7), where the axial velocity component u is given by the average of two values independently obtained by PTV). The second method is to check that the data of the velocity vector field obtained by Eq. (7) satisfies the continuity equation of axisymmetric flow. On the other hand, the present technique can be applied to flow fields that are not completely axisymmetric if only the mean flow is considered. For instance, in the presence of turbulence the system extracts the ensemble-averaged flow field for the axisymmetric mode. This can be shown by using Eq. (7) in a manner analogous to Reynolds decomposition. It requires substituting the mean and fluctuating contributions into the individual velocity components to confirm that, due to the linearity of the involved equations, the mean output velocities remain unmodified. In other words, any correlation terms containing fluctuating contributions vanish and do not affect the value of the calculated mean velocities.

Table 2
Summary of the experimental conditions for Taylor-Column.

		Large tank	Small tank	
Disk radius	R_d	25	25	(mm)
Rotational speed of tank	Ω	0.524	3.14, 4.71	(rad/s)
Rotational speed of disk	Ω_d	0.24–1.11	3.67–5.24	(rad/s)
Depth of tank from disk	H_1	>2000	230	(mm)
Depth of surface from disk	H_2	>100	50	(mm)
Rossby number	Ro	0.40–0.72	0.10–0.40	(–)
Light sheet thickness		5	3	(mm)
Light sheet off-set	ε	10	5	(mm)
Frame rate for PTV		7.5	60	(fps)
Shutter speed		7.5	60	(1/s)
Image size		640 × 480	1920 × 1080	(pixels)
Density of water (salty)		1.042×10^3	0.997×10^3	(kg/m^3)
Spatial resolution		0.086, 0.098	0.114	(mm/pixel)

3.2. Measurement results

We investigate three aspects of the flow around the sphere moving through the rotating liquid in the axial direction. Initially we present flow visualizations to illustrate the qualitative features of the wake behind the sphere as a function of the independent experimental parameters. Then we discuss quantitative data for the temporal evolution of the centre-line velocity components obtained from an in-plane PTV configuration. Finally we present three-dimensional vortical structures obtained from the off-axis PTV measurements.

3.2.1. Part 1: Qualitative visualization

Fig. 3 displays flow visualizations illustrating qualitative changes of the flow around the sphere in non-rotating and rotating environments for three different Reynolds numbers. The pictures show pathlines of tracer particles on the plane offset from the axis by $\varepsilon = 5$ mm. In the picture, the sphere moves from right to left (i.e. from bottom to top inside tank) and the vector of the background rotation, in Fig. 3(d–f) points to the left (i.e. upwards relative to tank). The vertical axis of the sphere is located behind the light sheet. Fig. 3(a–c) display the flow without background rotation. These three figures enable conceptualizing the existence of a single toroidal vortex behind the sphere that grows in the downstream direction as the Reynolds number increases. Background rotation fundamentally alters the wake structure as is illustrated by Fig. 3(d–f). For the case of rotating flow at the lowest Reynolds number, $Re = 0.5 \times 10^3$, Fig. 3(d) reveals the existence of a nearly stagnant flow region behind the sphere. The oblique path-lines in the stagnant region indicate that the flow induced within the wake is swirling relative to the background rotation. Since the vector of the background rotation points to the $+x$ direction and since local flow velocities near the surface at the rear of the sphere are towards the centerline one expects Coriolis forces inducing cyclonic swirling motion. This was observed in the experiments and the overall flow structure is reminiscent of a Taylor-Column. Comparison of Fig. 3(d and e) shows that radius of the region occupied by the cyclonic wake swirl narrows with the increase of Reynolds number. Finally, the swirling motion intensifies as is revealed by the longer diagonal pathlines.

3.2.2. Part 2: Velocity vector distribution

Fig. 4(a) shows a representative sample of our PTV data. The white circular region superposed onto the figure identifies the cross section of the sphere on the off-axis plane while the actual outline of the sphere is identified by the circle enclosing the central white region. Three-frame consecutive tracking of individual particles was applied to obtain the velocity vectors [15,2]. This algorithm is preferable to be employed for two reasons. One is the high out-of-plane velocity in the off-axis plane, particularly in the wake region. Another is a demand to reduce seeding number density of particles in the tank so that light scattering within the PTV plane is transmitted to the camera outside the tank. There are no PTV data measured in the dark shadow area of the light sheet and it is, consequently, omitted from the data analysis.

Fig. 4(b) shows the same instantaneous velocity vector distribution which is converted from scattered PTV data using the Laplace equation [14]. Here the scattered PTV data are used not only in space but simultaneously in time. This spatio-temporal interpolation allows us to reconstruct the flow field most realistically for PTV data of limited number density in space. The detailed performance of the technique was reported in one of our earlier papers [9].

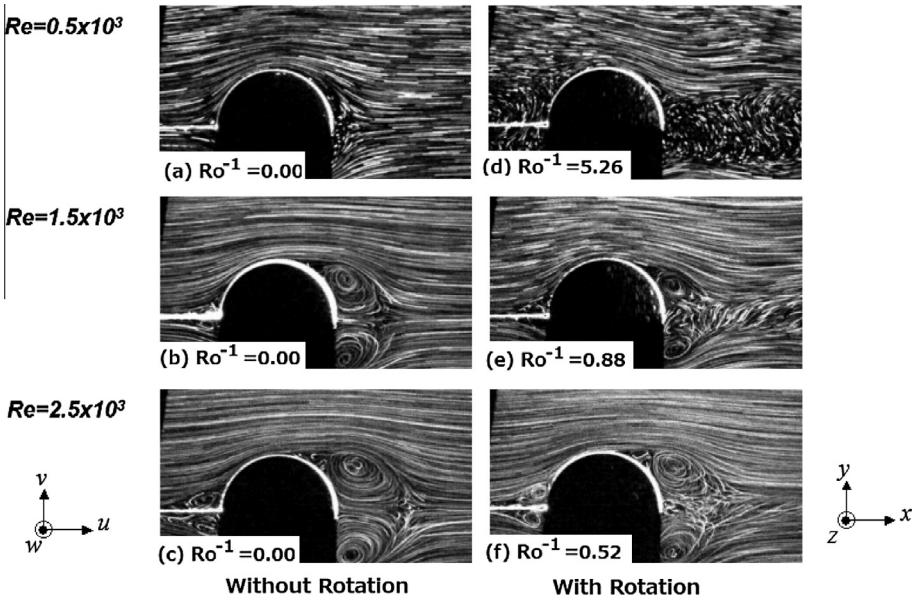

Fig. 3. Particle pathline visualization of flow around a sphere by off-axis light sheet illumination. The oblique path lines downstream of the sphere indicate the presence of a columnar wake spinning around the axis. From the top to the bottom, sphere speed is U = 10, 30, and 50 mm/s. Pictures in the right column are at the tank rotational speed of 5 rpm while those in the left at 0 rpm.

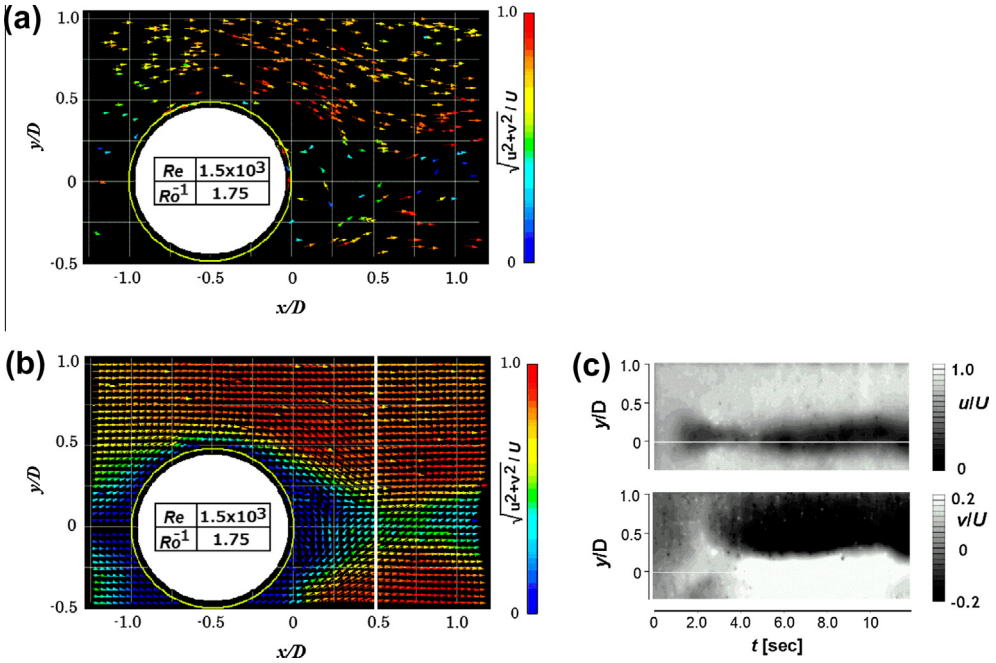

Fig. 4. Velocity information obtained within off-axis PTV plane. (a) Instantaneous velocity vector distribution obtained by PTV at the sphere speed of U = 30 mm/s and the rotational speed of 2.5 rpm. (b) Instantaneous velocity vector distribution interpolated by Laplace equation rearrangement. (c) Temporal evolution of two velocity components at x/D = 0.5.

Fig. 4(c) displays the temporal evolution of the u and the v components of the velocity after the sphere starts moving at t = 0 for an interval of twelve seconds. These are sampled in the direction of y/D, at the position x/D = 0.5 downstream of the sphere as indicated by the white line in Fig. 4(a).

The across-wake velocity distribution u/U indicates that the Coriolis force results in a stable stagnant region near the central axis. The velocity distributions for v/U along the across-wake direction y/D indicate that the wake adopts positive velocity on the central line y/D = 0 after $t \approx$ 3–5 s. This implies that local swirl exists near the central axis when Coriolis effects dominate. Fig. 4(c) reveals that, in this particular case, a steady flow state had been adopted approximately five seconds after the impulsive start of the sphere.

3.2.3. Part 3: Spatial development of swirl

From the in-plane PTV data, cross-sectional velocity fields in the y–z plane can be extracted at any required coordinate x/D upstream and downstream of the sphere. Fig. 5 displays examples of such cross-sectional velocity fields for the four different

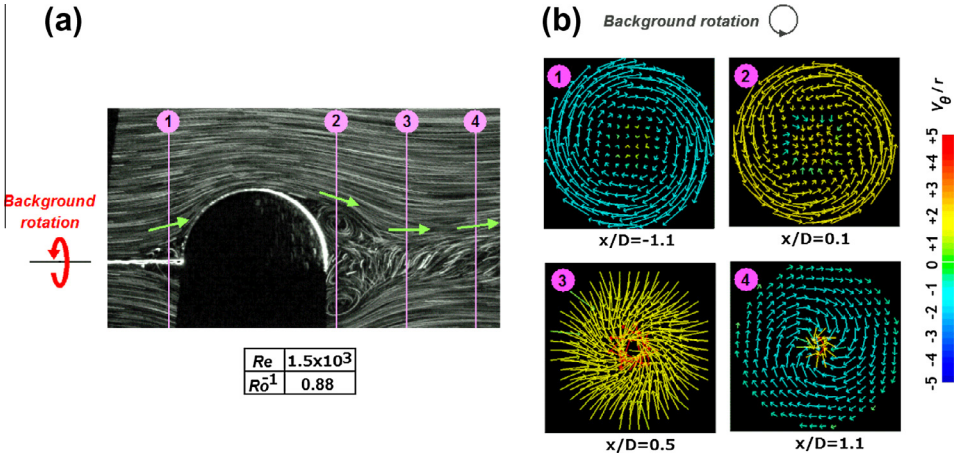

Fig. 5. Circumferential flow structure in four cross-sectional planes at $Re = 1.5 \times 10^3$, $Ro^{-1} = 0.88$ (the sphere speed is $U = 30$ mm/s at 5.0 rpm). Vector of rotational velocity points out of plane of paper; (1) induced anti-cyclonic swirl ahead of sphere, (2) acquisition of angular momentum outside the toroidal vortex, (3) free-vortex-type cyclonic swirl due to the throat effect of the stream, and (4) radial diffusion of axial vorticity in the downstream region.

locations, (1–4), identified in the figure. In the cross-sectional profiles the orientation of the vector of the rotational velocity **Ω** is pointing out of the plane of the paper, i.e. the sense of the background rotation is anti-clockwise. Cross section (1) shows a velocity field upstream of the sphere at $x/D = -1.1$. The flow field displays a weak anti-cyclonic swirl, i.e. clockwise in Fig. 5, relative to the background rotation. This sense of swirl of the flow ahead of the frontal stagnation point is expected. The vector of the rotational velocity in Fig. 5(a), and in the top part of Fig. 5(b), points to the left. Just ahead of the sphere and near to its surface there is a local flow velocity that is orientated radially outwards (i.e. from pole towards equator). Consequently the cross product of the two vectors just upstream of the sphere produces Coriolis forces that will act to induce an anti-cyclonic swirl. Just downstream of the sphere, in its wake, the situation is reversed since the local flow velocity near the sphere surface is orientated radially inwards. Here the swirl induced by the action of the Coriolis force is expected to be cyclonic. This sense of swirl in the wake is experimentally confirmed by our experimental PTV data for cross sections (2–4) where the flow is counter-clockwise; i.e. it has the same sense of rotation as the background rotation. A comparison of the velocity fields in cross-section (1) with those in cross sections (2–4) reveals furthermore that the wake swirl is more intense than the swirl ahead of the sphere. The comparison of the flow fields in cross-section (2 and 3) reveals that, for increasing distance x/D downstream of the sphere, the region of cyclonic swirl becomes increasingly confined to a central core surrounding the axis of rotation. This is consistent with the qualitative flow visualization above the cross-sectional profiles. Since the core region displays relatively low axial velocities compared to the fast circumferential rotation we refer to the wake as columnar.

3.2.4. Part 4: Three-dimensional visualization

Fig. 6 displays iso-surfaces of the three vorticity components, normalized by U/D, computed from the time-averaged velocity vector distribution. The averaging period is the interval from 7.0 s to 9.0 s after the impulsive start of the sphere, corresponding to 60 frames of PTV data. Over 1000 of the original PTV velocity vectors are used for this visualization. It is estimated that this is equivalent to a spatial resolution of around 1/10th of the sphere

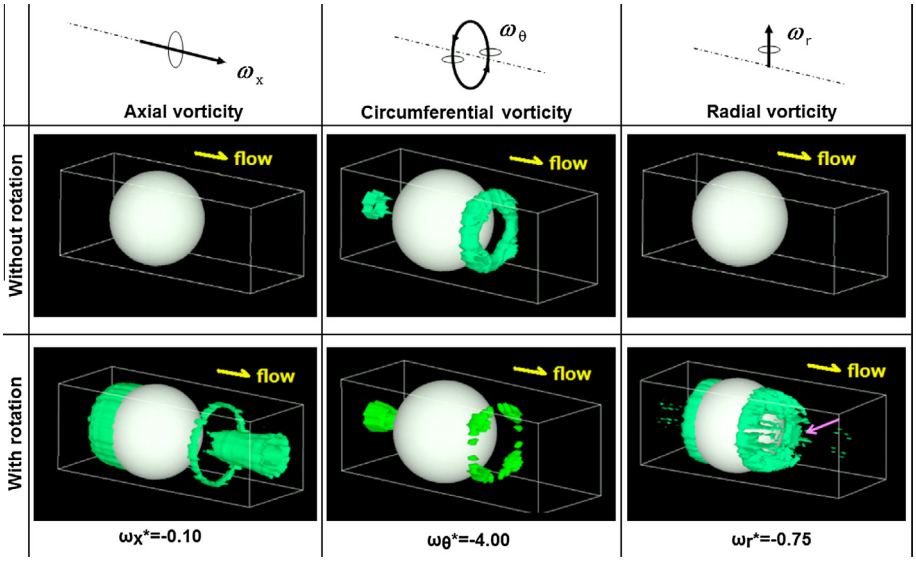

Fig. 6. Vorticity distributions normalized by U/D around the sphere for flow with and without background rotation at $Re = 1.5 \times 10^3$, $Ro^{-1} = 0.88$ ($U = 30$ mm/s, Ω is 5.0 rpm). Each value for iso-surface is shown at the bottom line.

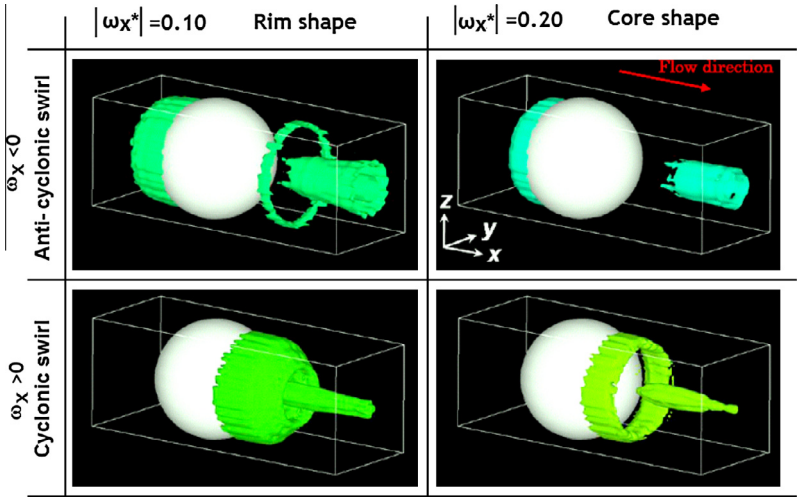

Fig. 7. Double-layer structure of the columnar wake visualized by iso-surfaces of different axial vorticities at $Re = 1.5 \times 10^3$, $Ro^{-1} = 0.88$. The sphere speed is 30 mm/s, and the rotational speed is 5.0 rpm.

diameter if a random distribution of velocity vectors is assumed. The axial vorticity ω_{x*} quantitatively corroborates that swirling motion around the rotational axis only exists when background system rotation is present. Comparison of the data in the presence and the absence of background rotation reveal a reduction of the circumferential vorticity component $\omega_{\theta*}$ for the rotating flow and it proves that background rotation suppresses the toroidal vortex formed behind the sphere in the non-rotating flow. Note that a ring of non-zero circumferential vorticity exists ahead of the sphere even in the absence of rotation. This non-zero upstream vorticity region is associated with a vortex that is formed due to the presence of the thread towing the sphere. The thread is clearly visible in the photos in Fig. 3 and the vertical structure near the thread can be identified in Fig. 3(b) and, more pronounced, in Fig. 3(c). The radial vorticity in Fig. 6 does not exist in the absence of background rotation. The source of radial vorticity is a gradient $\partial v_\theta/\partial x$ of the circumferential flow velocity along the x axis, and it implies the presence of the velocity gradient in the wake of the sphere.

Fig. 7 displays iso-surfaces for four different negative and positive values of the axial vorticity component ω_{x*}. The time-averaging period is the same as for the previous case. Similarly to Fig. 5, it reveals the existence of an upstream flow region displaying anti-cyclonic swirling motion (negative vorticity) immediately ahead of the sphere and a thin kernel of cyclonic swirl (positive vorticity) along the central axis. Nevertheless, the figure also reveals the existence of an annular region of negative vorticity surrounding the central cyclonic core. Hence, the overall wake adopts a compound structure with a cyclonically swirling core that is surrounded by a columnar region of anti-cyclonic swirl. The main conclusion emerging from the above analysis of PTV data is that for the flow around the sphere, the background rotation results in the generation of substantial axial and radial vorticity components ω_{x*} and ω_{r*} as well as in reduction of azimuthal component $\omega_{\theta*}$, associated with the presence of a toroidal vortex behind the sphere in the non-rotating case.

4. Taylor-Column moving in three dimensions

Immersing a differentially rotating disk in rotating fluid generates a Taylor-Column. Depending on the relative rotation of the disk to the ambient fluid, a variety of flow structures are observed both in the near and the far regions of the disk. In the near region, the Ekman layer on the disk surface drives the radial flow which also induces axial flow along the rotating axis, and forms a meridional circulation. If a sufficiently high shear rate is induced between the Taylor-Column and the ambient region, the column becomes unstable and adopts non-circular shapes (Hide and Titman, 1966). Such a flow structure is characterized by the following two dimensionless parameters, i.e. Rossby number and Ekman number.

$$Ro = \frac{\omega}{\Omega}, \quad Ek = \frac{\nu}{R_d^2 \Omega}, \quad \omega = \Omega_d - \Omega. \tag{11}$$

Here Ω_d and Ω are angular velocities of the disk and the tank, respectively. R_d is the disk radius, and ν is kinematic viscosity of fluid.

4.1. Pathline visualization and PTV measurement

Fig. 8 shows particle pathlines visualized by a laser sheet that is projected in the plane perpendicular to the rotational axis, i.e. flow visualization in the y–z plane (see Fig. 1(b) for the definition of coordinate system). The images are taken by a camera mounted on the frame of rotating tank, thus, the particle pathlines show the flow component induced by the presence of the disk. In these images, Taylor Column is unstable and forms non-circular shapes. Their shapes slowly rotate in the negative direction relative to the background rotation. Although the cross sectional shapes are clearly understood, the information on the axial velocity distribution, $u(x,y,z)$, is not obtained with this visualization.

Fig. 9 shows the vertical laser sheet visualization using off-axis illumination. The details of the experimental conditions are summarized in Table 2. The off-axis illumination allows us to detect the circumferential velocity component as the horizontal displacement of the particle. The vertical displacement in the image indicates the presence of the axial velocity component which increases with Rossby number. Fig. 10 shows samples of instantaneous velocity-vector distributions obtained within the off-axis measurement plane. The spatial distributions of PTV data are similar to the particle distributions shown in Fig. 9. These samples are selected from the case with high Rossby number, $Ro = 1.11$, where meridional circulation is induced inside the Taylor Column. As shown in the figure, the vertical flow component is induced both in the near field and the far field. The figure also reveals that the magnitude of the in-plane-velocity of the flow, which is projected onto the off-axis plane, is less than 15% of the primary circumferential velocity in the y direction so that the off-axis PTV has enough

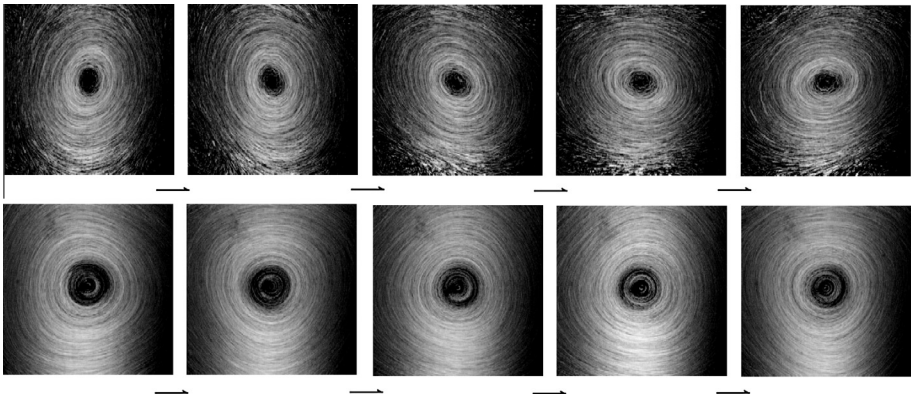

Fig. 8. Rotation of asymmetric Taylor Column visualized by particle pathlines in a small tank. Top figures represent ellipsoidal column for $Ro = 0.154$ and $Ek = 1.08 \times 10^{-4}$. Bottom figures are for triangular column for $Ro = 0.105$ and $Ek = 7.22 \times 10^{-5}$. Time interval of consecutive images is adjusted to be 1/12 of each rotating period.

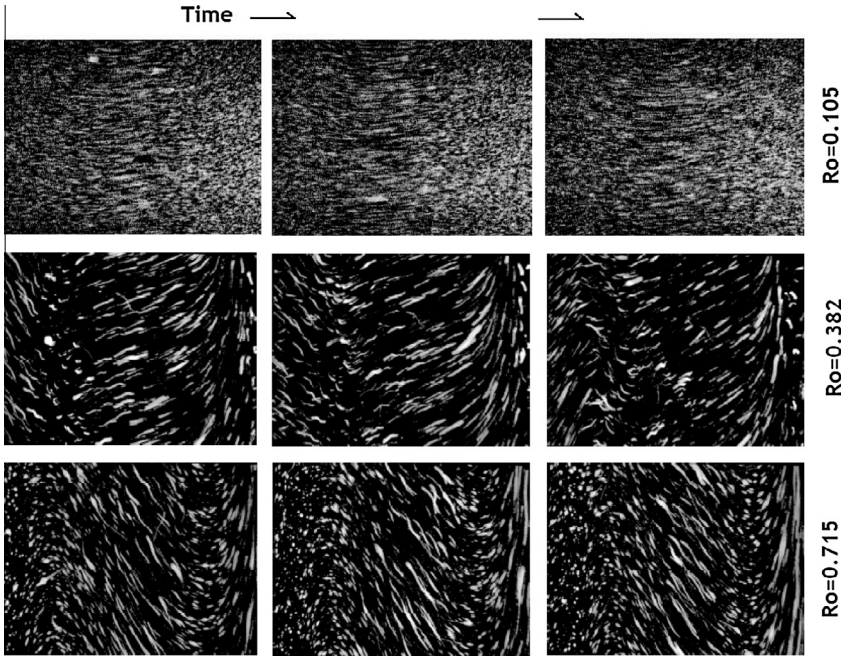

Fig. 9. Particle pathlines visualized in off-axis PTV plane. Three consecutive images have the time interval at 1/6 of the structure's rotating period on each condition of Rossby number. Top figures at $Ro = 0.105$ were visualized in a small tank, and the others were in a large tank.

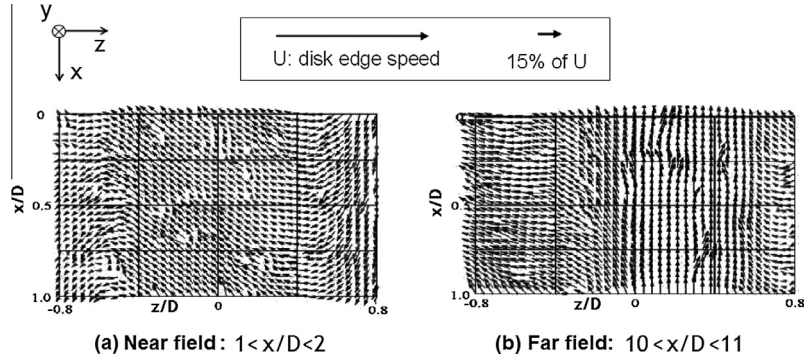

Fig. 10. Samples of instantaneous velocity vector distributions obtained in two off-axis PTV planes at different axial locations for $Ro = 1.11$, and $Ek = 3.05 \times 10^{-3}$ using a large tank.

sensitively to measure the secondary flow components that take place in the x–z plane.

4.2. Extension of Off-axis PTV to non-axisymmetric flow measurement

When the off-axis PTV is applied for non-axisymmetric flows such as for ellipsoidal and triangular columns, what can we obtain? While it cannot be suitably applied for completely unsteady 3-D flows, the off-axis PTV technique can be extended such that it can be applied to periodic flow structures in the azimuthal direction of the rotating system. Fig. 11 illustrates the geometrical relationship between the off-axis PTV plane and the rotating flow structure. By observing the rotating flow structure within the same rotating frame, the flow structure can be treated as steady while the off-axis PTV plane rotates as shown in Fig. 11(a). Namely, the flow structure can be scanned in the angular direction with many sets of PTV planes. Furthermore cross-points arise on which two PTV planes cross with each other. On these cross points, velocity vector of the flow is obtained from the data acquired in the two PTV planes as illustrated in Fig. 11(b). The equation for the velocity vector computation is given by

$$\mathbf{v} = \begin{pmatrix} v \\ w \end{pmatrix} = \frac{1}{\cos\theta_1 \sin\theta_2 - \cos\theta_2 \sin\theta_1} \begin{pmatrix} u_1 \sin\theta_2 - u_2 \sin\theta_1 \\ u_2 \cos\theta_1 - u_1 \cos\theta_2 \end{pmatrix}, \tag{12}$$

where v and w are the two velocity components in y–z plane on the frame that rotates with the same angular velocity as the rotating flow structure. θ_1 and θ_2 are the angles of the PTV planes relative to the rotating coordinate. u_1 and u_2 are the velocity components measured in individual PTV planes. On the cross points, the axial velocity components, u, measured in two PTV planes, should take the same value but may contain a small discrepancy due to PTV resolution, and it is corrected to be their mean value as

$$u = \frac{1}{2}(u_1 + u_2). \tag{13}$$

With these computations, the velocity vector distribution (u,v,w) is obtained in the whole field (x,y,z) as illustrated in Fig. 11(c).

The rotational speed of the PTV plane relative to the rotating flow structure is determined by the angular traveling velocity of the flow structure. Thus, the number of the PTV planes counted during a single rotation of the flow structure varies with the flow conditions. The angular velocity of the rotating flow structure can be obtained from data processing of velocity fluctuation in time. Fig. 12 shows the schematic principle to measure the angular velocity. As illustrated in Fig. 12(a), when a flow element migrates in the azimuthal direction, it produces two similar velocity fluctuations on the points, A and B, in the same PTV plane with a time lag. By analyzing the time lag, τ, the angular velocity of the rotating flow structure is obtained as

$$\Omega_f = \frac{\theta}{\tau} = \frac{1}{\tau} \sin^{-1}\left(\frac{2d}{\varepsilon}\right), \quad \because d = \varepsilon \sin\frac{\theta}{2} \tag{14}$$

where θ, d, and ε are the angle of the two points respect to the rotating axis, the distance from the centerline in the PTV plane, and the off-axis displacement (see Fig. 11(b)).

Fig. 12(b) shows the temporal fluctuation of the in-plane velocity profile, $v(y,t)$ in the case that a periodic structure passes the off-axis PTV plane. The time lag, τ, is obtained by auto-correlation analysis of the velocity data. When the temporal sampling interval of PTV, Δt, relative to τ is insufficient, reconstruction of the flow field becomes difficult. In such a case, the spatial number density of the cross points is lacking, for which Eqs. (12) and (13) are applied. Therefore, the applicability of the present extension of the off-axis PTV is guaranteed only when the angular velocity is lower than a critical value that is estimated by

$$\Omega_f < 0.1 \times \frac{2\pi}{\Delta t} = 0.2\pi F_r \tag{15}$$

where F_r is the sampling frequency of the off-axis PTV. If this condition is not satisfied, the sampling frequency should be increased. The underlying idea is essentially equivalent to adopting Taylor's frozen hypothesis, as applied in this study for the reconstruction of flow structures in the angular direction.

4.3. Error factors in flow field reconstruction

Availability of the present method of flow field reconstruction is restricted by several factors. Firstly, there is a phenomenological error factor, which is departure from the azimuthal periodicity of the flow itself. Irregular events in flow such as turbulent eddies cannot be reconstructed since such eddies behave chaotic. However, the secondary flow with azimuthal periodicity will be preserved in the measurement data. Thus, we can understand that

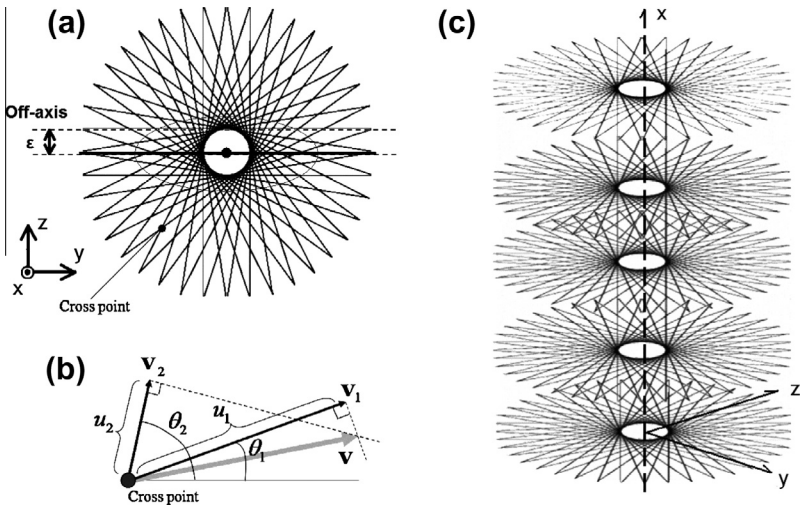

Fig. 11. Generation of cross points when flow structure rotates relatively to off-axis PTV plane, which are used to reconstruct non-axisymmetric velocity vector field. (a) Rotation of off-axis PTV planes in a horizontal cross section, (b) projection of flow velocity vector $\boldsymbol{u}$ onto two PTV planes, $\boldsymbol{u}_1$ and $\boldsymbol{u}_2$, on the cross point, and (c) vertical expansion for reconstruction of three-dimensional velocity vector field.

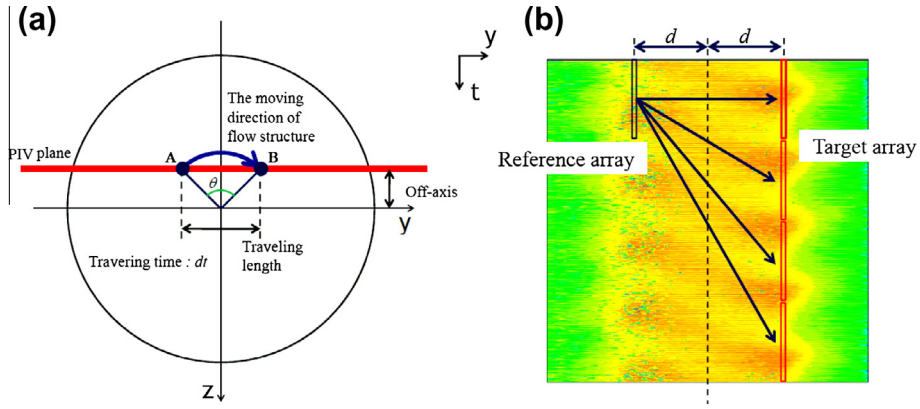

Fig. 12. Detection of periodic velocity fluctuations in off-axis PTV plane. (a) Two points defined along off-axis PTV plane, and (b) a sample of spatio-temporal velocity fluctuation measured on PTV plane, which is used to find out the circumferential traveling velocity of the flow structure from cross correlation analysis between two points.

the present method extracts the flow mode of the azimuthal periodicity when it is applied for a flow that includes both periodic and non-periodic flow structure. Hence, this is the same as phase-averaging technique known for complex wave form analysis. The second error factor is the lack of velocity data in the region around the rotating axis due to the off-axis displacement the PTV plane, ε. The smaller the off-set, the narrower the region of missing data is, however the azimuthal velocity distribution would be difficult to measure. Two-dimensional linear interpolation of the velocity is applied for the region with no velocity data, assuming the existence of a rigid vortex. The third error factor is spatial sampling interval of the PTV planes in the azimuthal direction. As the interval angle is expanded, the number of cross points for velocity vector computation decreases.

In order to confirm the basic characteristics respect to the above-mentioned error factors, we evaluated the flow field reconstruction performance numerically using an artificially synthesized non-axisymmetric vortex. Fig. 13 shows the results of the performance test: (a) is for change of off-axis length, and (b) is for the number of PTV planes in a single rotation of flow structure. The velocity vector figure in (a) is the artificially synthesized vortex model adopted for examination. In both figures, the ordinate is cross correlation of velocity vector field between the original velocity vector field, $\mathbf{u}_1$, and the reconstructed velocity vector field, $\mathbf{u}_2$, defined by

$$C_v = \frac{\int\int \mathbf{u}_1 \cdot \mathbf{u}_2 dxdy}{\sqrt{\int\int |\mathbf{u}_1|^2 dxdy \cdot \int\int |\mathbf{u}_1|^2 dxdy}}. \quad (16)$$

The data in Fig. 13(a) indicate that the off-axis length normalized by the disk radius at less than 0.5 maintains high reconstruction performance. Beyond the value, it is suddenly worsened because non-rigid rotational field enters the target of velocity vector interpolation. Another data shown in Fig. 13(b) proves that the increase in the number of PTV planes raises the reconstruction performance. At least 25 PTV planes should be provided for rough estimation of the flow structure with a cross-correlation of 0.8.

4.4. Measurement results

The experimental conditions are summarized in Table 2. The experimental study was conduced in a wide range of parameters with different combinations of rotational speeds of the disk and the tank. A variety of Taylor Column structures have been observed, and some of them need deep discussion in physical interpretation. In this paper we select to show a few test cases for demonstration purpose of the measurement technique.

Fig. 14 shows velocity vector fields of the Taylor Column measured at three locations from the rotating disk at $Ro = -1.17$, $Ek = 1.68 \times 10^{-3}$; 300 PTV frames were used for the reconstruction. On this condition, the column does not show significant azimuthal waves, and maintains an axisymmetric steady flow structure. The color indicates the axial velocity distribution which takes positive value inside the core and negative outside the column. It proves the presence of meridional circulation which is the well known internal circulation in the Taylor Column. The magnitude of the axial velocity due to the meridional circulation increases with the

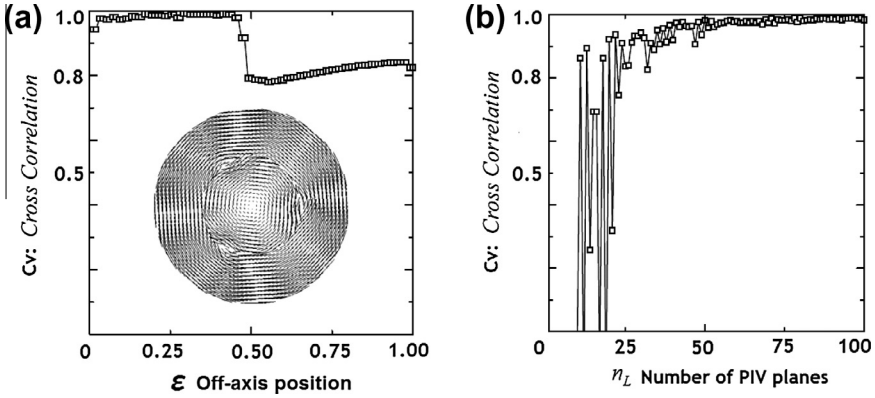

Fig. 13. Numerical reconstruction performance of non-axisymmetric velocity vector field, evaluated by vector cross correlation coefficient. (a) Influence of off-axis length relative to the radius of columnar structure. (b) Influence of number of PTV planes in a cycle, which depends on traveling angular velocity of flow structure relative to rotating tank.

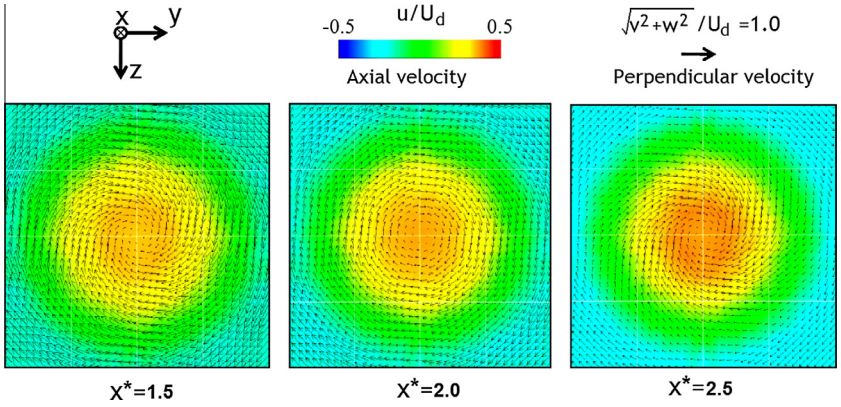

Fig. 14. Three-dimensional velocity vector field obtained at three different axial positions for $Ro = -1.17$, $Ek = 1.68 \times 10^{-3}$. Arrows show the flow velocity vector in y–z plane while color indicates the distribution of axial flow in x direction. The velocity vector field is reconstructed from the data of 300 PTV frames.

distance x^* from the disk, and it agrees with conventional understanding.

Fig. 15 shows three-dimensional velocity vector distributions for positive but small Rossby number cases. The number of PTV frames used for the reconstruction is 256, during which the off-axis PTV plane experiences five passages of azimuthal structures. In these cases, azimuthal structures appear: (a) represents an ellipsoidal column measured at $Ro = 0.154$ and $Ek = 1.08 \times 10^{-4}$ and (b) represents a triangular column at $Ro = 0.105$ and $Ek = 7.22 \times 10^{-5}$. Presence of such non-axisymmetric modes was found by Hide and Titman (1966) with dye visualization, and numerically by Hollerbach [8]. We confirmed the same structure with our PTV technique. In dye visualization, such azimuthal structuring of the flow is observed with intermediate process of dye transport. The present technique enables assessing the structure with physical dimension based on velocity as discussed below.

Fig. 16 shows a finer depiction of the triangular column sliced in y–z plane, which was measured for $Ro = 0.105$ and $Ek = 7.22 \times 10^{-5}$. The velocity vector distribution shown in (a) clearly proves counter clockwise rotation of fluid inside the column, which is

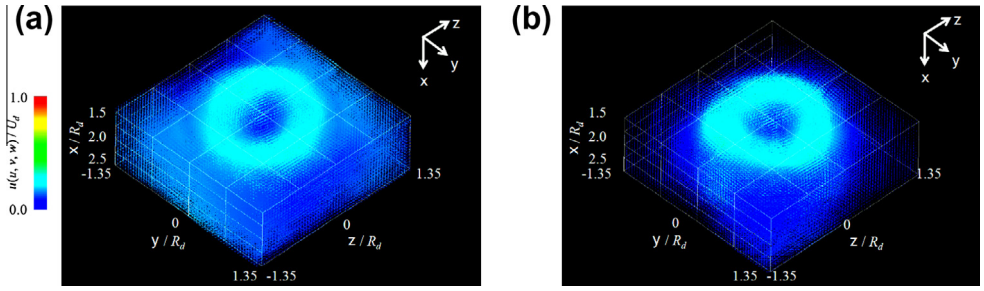

Fig. 15. Overviews of three-dimensional velocity vector distributions measured by the present off-axis PTV technique. (a) Ellipsoidal column measured at $Ro = 0.154$ and $Ek = 1.08 \times 10^{-4}$. (b) Triangular column measured at $Ro = 0.105$ and $Ek = 7.22 \times 10^{-5}$. In both cases, 256 PTV frames are used for reconstruction.

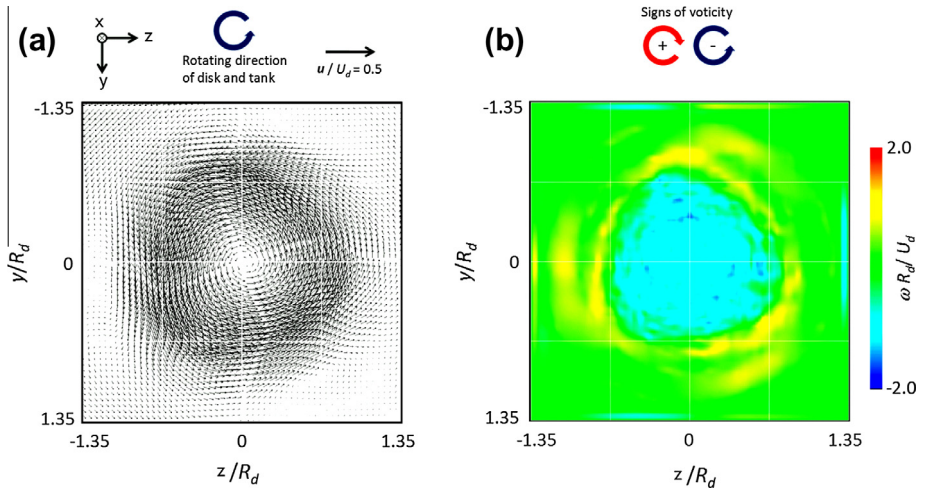

Fig. 16. Cross sectional flow structure of Taylor column on triangular mode at $Ro = 0.105$ and $Ek = 7.22 \times 10^{-5}$. (a) Velocity vector field relative to rotating tank, and (b) axial vorticity distribution from which a radial combination of cyclonic core and anti-cyclonic layer can be identified similarly to the sketch of Hide and Titman at $M = 3$.

induced in the same direction as the background rotation. While the core part of the column consists of a rigid rotational velocity field, the outer rim takes the highest velocity with triangular stream. By computing the vorticity it is found that the column is organized into vortical structures with different signs as shown in (b). The region of negative vorticity in blue has triangular shape, and it is surrounded by a thin layer of positive vorticity in yellow color. Just near the individual apex of the triangular rim, isolated segment of positive vorticity is observed.

In fact, we have also found more remarks with these data analysis, such as persistency of such non axisymmetric structure in the axial direction, and phase lag of rotation. We would like to report on the further fluid dynamics discussion for such data sets in a separate paper in the future.

5. Conclusions

We have described the first PTV measurements investigating the three-dimensional flow field established when a sphere propagates through a rotating fluid along the axis of rotation. We have used a single off-axis light sheet to obtain PTV data by means of a single camera, which enabled the reconstruction of the columnar flow formed behind the sphere. By choosing a regime where the inertial and Coriolis forces compete with each other, i.e. Rossby number around unity, the main observations were that background rotation results in the collapse of the toroidal vortex that exists just downstream of the sphere in non-rotating flow. Moreover, background rotation establishes an anti-cyclonic swirling motion ahead of the translating sphere and a cyclonic wake swirl that forms while the sphere translates through the fluid. The wake of the sphere was observed to display a compound structure consisting of a columnar cyclonically swirling core surrounded by an annulus with anti-cyclonic flow.

In the second half of the paper, we expanded the off-axis PTV technique to non axisymmetric flow measurement which is available for the flow in azimuthal periodicity. It is applied for investigation of Taylor Column that shows a variety of 3-D velocity distribution dependent on the combination of two rotational speeds of the disk and the tank. Some of typical flow structures have been successfully measured not only for the ordinary circular Taylor Column, but also for non axisymmetric columns accompanying ellipsoidal and triangular cores.

In summary, expected functions of the present off-axis PTV have been fairly confirmed with two kinds of experimental demonstrations for columnar flows which are formed in rotating background. Their measurements realized 3-D visualization of flow structures on the basis of velocity vector field information. Further details of the flow structures in many parametric combinations will be positioned as our future in-depth investigations.

References

[1] E. Achenbach, Vortex shedding from spheres, J. Fluid Mech. 62 (1974) 209–221.
[2] R.J. Adrian, Twenty years of particle image velocimetry, Exp. Fluids 39 (2005) 159–169.
[3] M.A. Brend, P.J. Thomas, Decay of vortex rings in a rotating fluid, Phys. Fluids 21 (2009) 044105-1–044105-4.
[4] B. Cushman-Roisin, Introduction to Geophysical Fluid Dynamics, Prentice-Hall, Englewood Cliffs, New Jersey, USA, 1994.
[5] M.R. Foster, R.J. Munro, The linear spin-up of a stratified, rotating fluid in a square cylinder, J. Fluid Mech. 712 (2012) 7–40.
[6] H.P. Grennspan, The Theory of Rotating Fluids, Cambridge University Press, Cambridge, UK, 1968.
[7] R. Hide, C.W. Titman, Detached shear layers in a rotating fluid, J. Fluid Mech. 29 (1966) 39–60.
[8] R. Hollerbach, Instabilities of the Stewartson layer. Part 1. The dependence on the sign of Ro, J. Fluid Mech. 492 (2003) 289–302.
[9] T. Ido, T.Ido.Y. Murai, F. Yamamoto, Post-processing algorithm for particle tracking velocimetry based on ellipsoidal equations, Exp. Fluids 32 (2002) 326–336.
[10] S. Lee, A numerical study of the unsteady wake behind a sphere in a uniform flow at moderate Reynolds numbers, Comput Fluids 29 (2000) 639–667.
[11] T. Leweke, M.C. Thompson, K. Hourigan, Instability of the flow around an impacting sphere, J. Fluids Struct. 22 (2006) 961–971.
[12] T. Maxworthy, The observed motion of a sphere through a short, rotating cylinder of fluid, J. Fluid. Mech. 31 (1968) 643–655.
[13] T. Maxworthy, The flow created by a sphere moving along the axis of a rotating slightly-visous fluid, J. Fluid Mech. 40 (1979) 453–479.
[14] Y. Murai, T. Ido, F. Yamamoto, Post-processing method using ellipsoidal equations for PTV measurement results: extension to unsteady flow, JSME Int J B 45 (2002) 142–149.
[15] K. Nishino, N. Kasagi, M. Hirata, Three-dimensional particle tracking velocimetry based on automated digital image processing, J. Fluids Eng. 111 (1989) 384–391.
[16] A.K. Norman, E.C. Kerrigan, B.J. McKeon, The effect of small-amplitude time-dependent changes to the surface morphology of a sphere, J. Fluid Mech. 675 (2001) 268–296.
[17] J. Proudman, On the motions of solids in a liquid possessing vorticity, Proc. R. Soc. Lond. A 92 (1916) 408–424.
[18] R.K. Reddy, J.B. Joshi, K. Nandakumar, P.D. Minev, Direct numerical simulations of a freely falling sphere using fictitious domain method: breaking of axisymmetric wake, Chem. Eng. Sci. 65 (2010) 2159–2171.
[19] H. Schlichting, Boundary-layer Theory, Springer-Verlag, Berlin, Germany, 1999.
[20] G.I. Taylor, Experiments on the motion of solid bodies in rotating fluids, Proc. R. Soc. Lond. A 104 (1923) 213–219.
[21] D.J. Tritton, Physical Fluid Dynamics, Oxford University Press, Oxford UK, 1988.
[22] J.P. Vanyo, Rotating Fluids in Engineering and Science, Dover Publications, Mineola, New York, USA, 2001.